Nucleation of Graphene and its Conversion to Single Walled Carbon Nanotubes

Matthieu Picher[1,2,†], Pin Ann Lin[1,2,†], Jose L. Gomez-Ballesteros[3], Perla B. Balbuena[3], and Renu Sharma[1]*

[1]Center for Nanoscale Science and Technology, National Institute of Standards and Technology, Gaithersburg, MD 20899-6203, USA

[2]University of Maryland – IREAP, College Park, MD 20742, USA

[3]Department of Chemical Engineering, Texas A&M University, College Station, TX 77843

[†]The first two authors contributed equally to this work.

KEYWORDS: Carbon Nanotubes, Graphene, nucleation mechanism, Environmental Transmission Electron Microscopy, Atomic Scale Observation.

ABSTRACT: We use an environmental transmission electron microscope to record atomic-scale movies showing how carbon atoms assemble together on a catalyst nanoparticle to form a graphene sheet that progressively lifts-off to convert into a nanotube. Time-resolved observations combined with theoretical calculations confirm that some nanoparticle facets act like a vice-grip for graphene, offering anchoring sites, while other facets allow the graphene to lift-off, which is the essential step to convert into a nanotube.

TEXT: Single-walled carbon nanotubes (SWCNTs) continue to be one of the most desirable materials for nanotechnology device integration.[1] For example SWCNTs exhibit high on/off current ratios, large charge carrier mobilities and high current carrying capacity making them ideally suitable for making nanoscale transistors.[2, 3] Yet limited SWCNTs based technologies have emerged on the market because of the lack of control on the structure of SWCNTs, i.e., diameter, defect density, length and chiral angle. During SWCNTs growth, the nucleation step, which sets the stage for the addition of subsequent atomic building blocks, is crucial because the precise arrangement of carbon atoms controls their opto-electronic properties.[4] Theoretical simulations have shown that during carbon nanotube synthesis by catalytic chemical vapor deposition (C-CVD), the carbon precursor is decomposed on the catalyst surface generating carbon atoms that assemble first into a graphene nucleus via sp^2 hybridization.[5] The graphene nucleus then propagates on the catalyst nanoparticle surface and progressively wraps around the nanoparticle surface converting into a hemispherical cap via incorporation of carbon pentagons in the initial honeycomb structure.[6-8] The structure of the cap at the time of its lift-off determines the chirality of the SWCNT, which should remain the same as more carbon atoms are added to the tubular structure, as long as the thermodynamic conditions do not change.[9, 10]Although these simulations provide a fundamental framework for nanotube growth,[11-13] they lack connectivity to

experimental growth conditions. For example, most of the simulations are performed on a free-standing catalyst particle, ignoring the catalyst-support interactions, and at a significantly higher temperature compared to the typical C-CVD experimental conditions. Moreover, *in situ* atomic scale observations have elucidated some salient features of carbon nanotube growth that were in direct conflict with theoretical predictions, e.g. nanotubes grow from solid particles,[14, 15] the structure of catalyst particle can be metal carbide.[16, 17] Therefore direct atomic scale observations are needed to elucidate the nucleation and growth process of single walled carbon nanotubes under growth conditions.

The main challenge for direct imaging of nucleation is that it involves a small number of atoms and a short time scale, and thereby requires a combination of high spatial and temporal resolution. We have overcome this constraint by reducing the growth rate to harmonize with the temporal resolution of our recording media. We have employed an environmental scanning transmission electron microscope (ESTEM),[18] equipped with an image corrector and a digital video recording system, to follow SWCNT growth using a low pressure of acetylene (C_2H_2) as the carbon source and a Co-Mo/MgO catalyst (Materials and Methods in Supporting information).Ref Figure 1 shows time resolved high resolution images extracted from a video (Supporting information Movie S1) recorded at a frame rate of 6 s^{-1} at 625 °C in 0.005 Pa of C_2H_2. A number of nanoparticles, ranging from 1 nm to 2.5 nm in size, oriented along low index zone axes on MgO are visible within a recorded 20 nm x 20 nm area. Most of these nanoparticles were active for nanotube growth (Supporting information Movie S1). Two-dimensional lattice resolution in most of the particles, marked as P1 and P2 in Figure 1 and P3, P4, P5 and P6 in Supporting Information Figure S2, is maintained throughout the observation period of 104 s. At the start of our video recording (Time = 0 s) the structures of P1 and P2 were Co_3C and CoO,

respectively, as determined from the Fast Fourier transforms (FFT) of the images (Materials and Methods and Figure S1 in Supporting Information). After 58 s, P1 converted into Co_2C, a carbon richer phase and P2 converted into Co_3C (Figure 1b).[19] This transition of metal oxide to metal carbide indicates that P1 may have converted to Co_3C before we started recording the video. In general all nanoparticles converted to Co_2C structure before nanotube nucleation. Iron carbide formation during carbon nanotube growth has been previously observed,[16, 17] but similar direct evidence for cobalt carbide had not been reported. A number of other particles, active for CNT growth (Figure S2, S3 and Table S2) were also measured to ensure the structure identification of active particles as the structures of Co_3C and Co_2C are very similar and undistinguishable in certain orientations. These measurements confirmed Co_2C structure as the active phase for nanotube nucleation here.

Although the nominal composition of the catalyst contains Mo[20] which was confirmed by energy dispersive x-ray analysis and electron energy-loss spectroscopy of large catalyst/support areas but we did not find any Mo in active catalyst particles. Therefore we do not have direct experimental evidence to decipher the exact role of Mo for SWCNT growth.

Higher magnification images, extracted from Supporting Information Movie S2, of nanoparticle marked as P2 in Figure 1 are shown in Figure 2. The Co_2C nanoparticle is orientated along the zone axis and is bound by {020} and {210} planes in projection (Figure 2a and 2e). We first observe a graphene embryo to nucleate on the corner of $Co_2C_{(020)}$ and $Co_2C_{(210)}$ surfaces (Figure 2a) and spread over the $Co_2C_{(210)}$ surface during the growth (Figure 2b). The observed bending of the growing graphene is proposed to be stabilized by the insertion of pentagons,[21] which is the first step in forming the hemispherical cap. The graphene is in close contact with $Co_2C_{(020)}$ surface but is slightly lifted from $Co_2C_{(210)}$ which is confirmed by the average measured distances

of (0.15 ± 0.01) nm* and (0.26 ± 0.01) nm* (Figure 2m). With its left side anchored to the $Co_2C_{(020)}$ surface, the lateral expansion occurs via atomic scale jumps of its right edge on $Co_2C_{(210)}$ (Figure 2b-d, f-h). This expansion of tube diameter may also be favored by the reduction of the curvature energy.[22] Once the graphene reaches the second $Co_2C_{(020)}$ surface, both sides are anchored to $Co_2C_{(020)}$ surfaces (Figure 2i,k). In a remarkable process, the incorporation of additional carbon atoms results in cap lift-off on the (210) plane and nanotube growth, while the sides stay anchored to the {020} surfaces. At this point, the nanotube cap structure is determined and the elongation starts with well-defined diameter and chiral angle (Figure 2j,l).[12] It is interesting to note that on {210} surface C atoms are separated by four Co atoms. Therefore a facet with less than four atoms may have only Co atoms and also provide anchoring point (Figure 2k).

The anchoring of graphene on $Co_2C_{(020)}$ and its detachment from $Co_2C_{(210)}$ surfaces observed here in the 2D images can be explained by density functional theory (DFT) calculations, where full 3-D nature of the graphene/nanoparticle interaction can be explored. The Co_2C {020} and {210} surfaces are identified as Co terminated and Co-C terminated, respectively (Materials and Methods, Figure S3 and Figure S4 in Supporting Information), which are reported to be stable terminations for these surfaces.[23] The distances between the graphene sheet and these two surfaces, and the corresponding work of adhesion values were calculated starting from the models as shown in Figure 3a and 3c. After relaxation, the graphene sheet is almost flat and in close contact with Co terminated {020} surface. The calculated distance between graphene and the nanoparticle ranges from 0.180 nm to 0.202 nm (Figure 3b). On the other hand, it forms a dome on Co-C terminated {210} surface with calculated distances of 0.191 nm on the edge and 0.309 nm at the center, respectively (Figure 3d). These values are in close agreement with

experimental measurements (Figure 2m). The calculated work of adhesion for graphene on Co terminated {020} surface is higher than for Co-C terminated {210} surface with corresponding values of adhesion to be -26.5 eV nm^{-2} and -14.4 eV nm^{-2}, respectively (Table S2 in Supporting Information). Therefore, the nanoparticle surface termination plays a critical role in determining the work of adhesion between graphene and the nanoparticle: a Co terminated surface favors graphene anchoring, providing a 'vice grip' like hold, while a Co-C terminated surface promotes graphene detachment and cap lift-off. In both simulation and experiment, the central part of the graphene sheet is observed to be lifted from the {210} surface, but the edge of the graphene sheet is maintained in close contact with {210} surface forming a convex-like structure. Despite a low work of adhesion, the growing structure remains attached at its edge. This can be explained by the presence of dangling bonds at the graphene edges which tend to bind with the nanoparticle to be stabilized.

In summary, we have illustrated how atomically resolved dynamic imaging, combined with theoretical calculations, provide essential insights into nanomaterial nucleation and growth process. We find that catalytically active nanoparticles possess adjacent surfaces with dissimilar works of adhesion for graphene. We propose that this disparity between facets is essential for CNT growth as it offers the necessary combination of anchoring and lift-off sites. This favors the conversion of the graphene nucleus into a nanotube and prevents nanoparticles from encapsulating, which is one of the major causes of catalyst deactivation and reduction in CNT synthesis yield.[24-26] These first atomic scale observations show that, since the nanotube cap structure and the diameter are controlled by nanoparticle facet geometry, the chirality will also be determined at this stage. In future this information can be used to design a catalyst/support system for large scale synthesis of single walled CNTs with pre-defined chirality. A prerequisite

for achieving this control is a strong catalyst/support interaction to preserve the distinct nanoparticle facets under growth conditions, as observed in our Co/MgO system. We believe that associating this type of catalytic system with a very narrow nanoparticle diameter distribution is essential for deterministically obtain SWCNTs with specific diameters and chiralities, and thus specific opto-electronic properties. Such experimental atomic resolution movies provide a consistent nano-scaled input for growth simulation models.

FIGURES

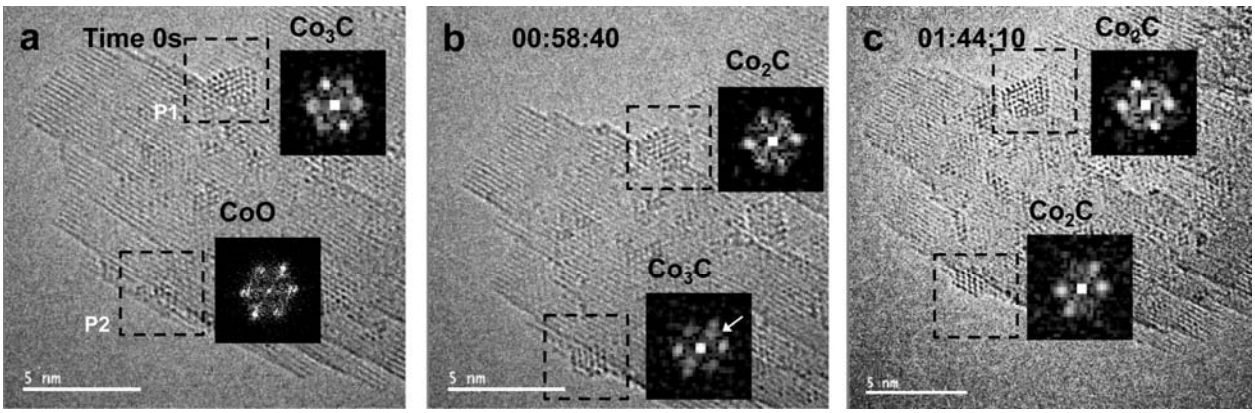

Figure 1. Structural transformation of catalyst nanoparticles after C_2H_2 introduction. (a, b, c) A series of high resolution images extracted from a digital video (Supporting Information Movie S1) recorded after introducing 0.005 Pa C_2H_2 at 625 °C. FFTs from the particles P1 and P2 regions (insets) are used for structure identification. Structure of P1 converted from Co_3C (a) to Co_2C (b) while P2 changed from CoO (a) to Co_3C (b) and then to Co_2C (c) before nucleating SWCNTs. The white arrow in FFT of particle P2 indicates the contribution from MgO support. Scale bars are 5 nm.

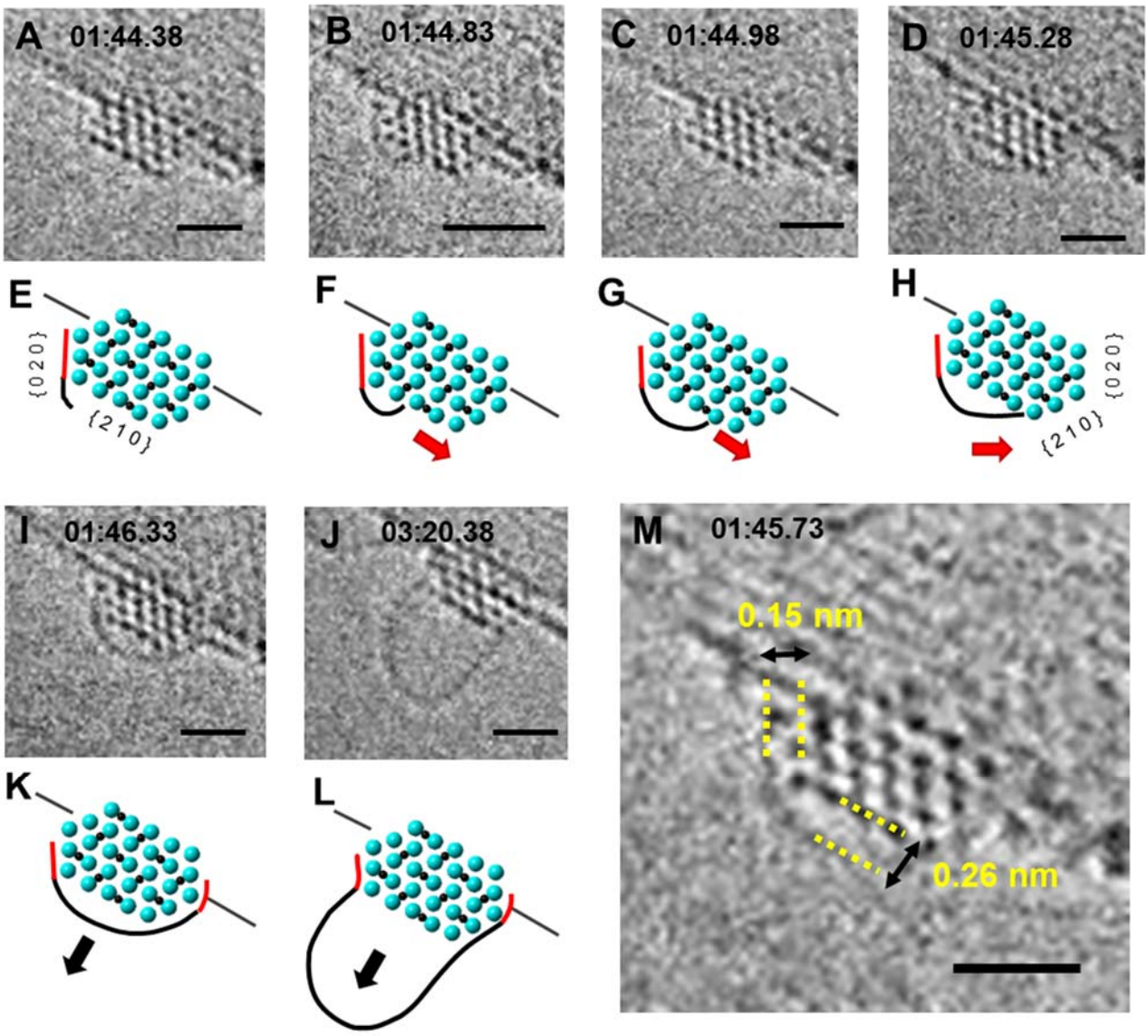

Figure 2. *In situ* time-resolved ETEM observation of SWNT nucleation and growth. (a, b, c, d) (i) (j) A series of images extracted from Supporting Information Movie S2 of a Co_2C showing SWCNT growth. (e, f, g, h) (k) (l) Corresponding atomic models. The active surfaces of the catalyst are identified to be {020}c and {210}. The red lines indicate the stronger adhesion between graphene and metal on the two $Co_2C_{(020)}$ surfaces and black line shows slightly lifted graphene from {210} surface that results in the formation of cap and growing SWCNT. The arrows are guiding the growth directions. (m) Snapshot showing the average distances between

the growing structure and the {020} and {210} catalyst surfaces before the nanotube lift-off. Scale bars are 1 nm.

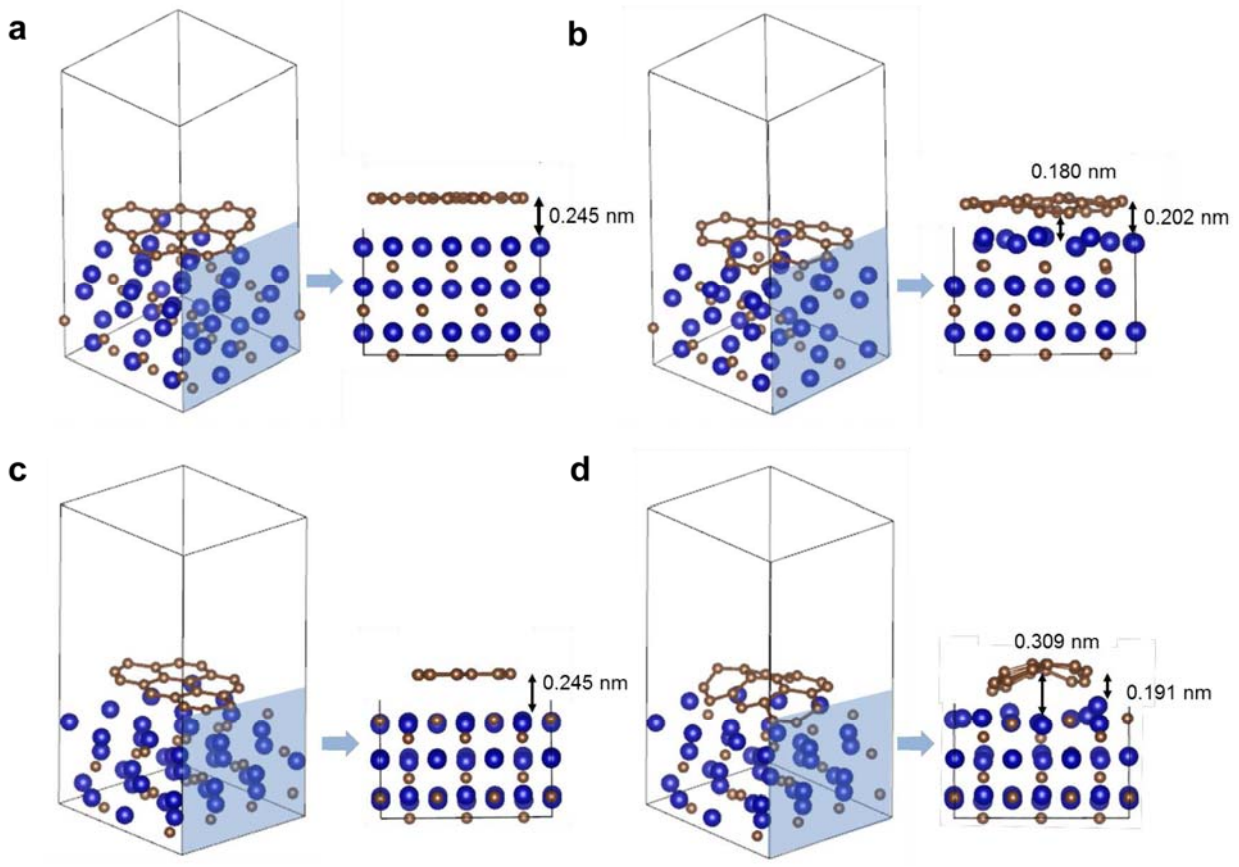

Figure 3. Models used in DFT simulation of graphene relaxation on $Co_2C_{(020)}$ and $Co_2C_{(210)}$ surfaces. (a) (c): Graphene sheets were initially placed at a distance of 0.245 nm from a Co terminated $Co_2C_{(020)}$ surface and at the same distance from a Co-C terminated $Co_2C_{(210)}$ surface, respectively. After relaxation of graphene on Co_2C surfaces, distance changes to 0.180 nm to 0.202 nm from $Co_2C_{(020)}$ (b) and to 0.191 nm to 0.309 nm from $Co_2C_{(210)}$ (d). These distances are in close agreement with the measured distance (Figure 2m). For each panel, a 3D view (left) and a side view (right) are proposed for visual clarity.

ASSOCIATED CONTENT

Materials and Methods, high resolution movies, supporting figures and tables; This material is available free of charge via the Internet at http://pubs.acs.org.

AUTHOR INFORMATION

Corresponding author

*Corresponding author. E-mail: Renu.sharma@nist.gov

Author Contributions

MP and PAL acquired and analyzed the movies, taking equal credit as first authors; JLGB and PBB made DFT simulations and RS supervised the experimental design, provided ideas for data analysis and simulations and contributed towards manuscript writing. All authors discussed the results and commented on the manuscript at all stages.

Notes

Disclaimer: In the full description of the procedures used in this document, certain commercial products and their suppliers are identified. The inclusion of such information should in no way be construed as indication that such products or suppliers are endorsed by NIST or are recommended by NIST or that they are necessarily the best materials, instruments, software or suppliers for the purposes described.

ACKNOWLEDGEMENT

Authors PBB and JLG-B gratefully acknowledge the support from the US Department of Energy, Basic Energy Sciences, under grant DE- FG02-06ER15836. Computational resources from TAMU Supercomputer Facility, Brazos Cluster at Texas A&M University, Texas

Advanced Computing Center (TACC), and from the National Energy Research Scientific Computing Center, which is supported by the Office of Science of the U.S. Department of Energy under Contract No. DE-AC03-76SF00098, are also gratefully acknowledged.

ABBREVIATIONS

Single-walled carbon nanotubes (SWCNTs), catalytic chemical vapor deposition (C-CVD), fast Fourier transforms (FFT), environmental scanning transmission electron microscope (ESTEM), density functional theory (DFT).

REFERENCES

1. De Volder, M. F. L.; Tawfick, S. H.; Baughman, R. H.; Hart, A. J. *Science* **2013,** 339, (6119), 535-539.
2. Wei, B. Q.; Vajtai, R.; Ajayan, P. M. *Applied Physics Letters* **2001,** 79, (8), 1172-1174.
3. Durkop, T.; Getty, S. A.; Cobas, E.; Fuhrer, M. S. *Nano letters* **2004,** 4, (1), 35-39.
4. Bachilo, S. M.; Strano, M. S.; Kittrell, C.; Hauge, R. H.; Smalley, R. E.; Weisman, R. B. *Science* **2002,** 298, (5602), 2361-2366.
5. Moors, M.; Amara, H.; Visart De Bocarmé, T.; Bichara, C.; Ducastelle, F.; Kruse, N.; Charlier, J.-C. *Acs Nano* **2009,** 3, (3), 511-516.
6. Shibuta, Y.; Maruyama, S. *Chemical physics letters* **2003,** 382, (3), 381-386.
7. Reich, S.; Li, L.; Robertson, J. *Chemical physics letters* **2006,** 421, (4), 469-472.
8. Gómez-Gualdrón, D. A.; Balbuena, P. B. *The Journal of Physical Chemistry C* **2008,** 113, (2), 698-709.
9. Yao, Y.; Dai, X.; Liu, R.; Zhang, J.; Liu, Z. *The Journal of Physical Chemistry C* **2009,** 113, (30), 13051-13059.
10. Arenal, R.; Lothman, P.; Picher, M.; Than, T.; Paillet, M.; Jourdain, V. *The Journal of Physical Chemistry C* **2012,** 116, (26), 14103-14107.
11. Ohta, Y.; Okamoto, Y.; Page, A. J.; Irle, S.; Morokuma, K. *ACS Nano* **2009,** 3, (11), 3413-3420.
12. Elliott, J. A.; Shibuta, Y.; Amara, H.; Bichara, C.; Neyts, E. C. *Nanoscale* **2013,** 5, (15), 6662-6676.
13. Tefera, A. G.; Mochena, M. D. *Carbon* **2014,** 67, 198-202.
14. Helveg, S., Lopez-Cartes, C., Sehested, J., Hansen, P.L.,Clausen, B.S., Rostrup-Nielsen, J.R., Abild-Pedersen, F., and Norskov J. *Nature* **2004,** 427, 426
15. Sharma, R., Zafar, Iqbal *Applied Physics Letters* **2004,** 84, 990-992.
16. Yoshida, H.; Takeda, S.; Uchiyama, T.; Kohno, H.; Homma, Y. *Nano Letters* **2008,** 8, (7), 2082-2086.
17. Sharma, R., Moore, E.S., Rez, P, Treacy M.M.J. *Nano Letters* **2009,** 9, (2), 689-694.
18. Sharma, R., Crozier, Peter A., Environmental Transmission Electron Microscopy in Nanotechnology. In *Transmission Electron microscopy for nanotechnology*, Wang, N. Y. Z. L., Ed. Springer-Verlag and Tsinghua University Press: 2005; pp 531-565.
19. Nagakura, S. *Journal of the Physical Society of Japan* **1961,** 16, 1213-1219.
20. Goyal, A.; Wiegand, D. A.; Owens, F. J.; Iqbal, Z. *Chemical physics letters* **2007,** 442, (4), 365-371.
21. Reich, S.; Li, L.; Robertson, J. *Physical Review B* **2005,** 72, (16).

22. Ribas, M. A.; Ding, F.; Balbuena, P. B.; Yakobson, B. I. *The Journal of chemical physics* **2009,** 131, (22), 224501.
23. Zhao, Y.-H.; Su, H.-Y.; Sun, K.; Liu, J.; Li, W.-X. *Surface Science* **2012,** 606, (5–6), 598-604.
24. Yamada, T.; Maigne, A.; Yudasaka, M.; Mizuno, K.; Futaba, D. N.; Yumura, M.; Iijima, S.; Hata, K. *Nano Letters* **2008,** 8, (12), 4288-4292.
25. Picher, M.; Anglaret, E.; Arenal, R.; Jourdain, V. *Nano letters* **2009,** 9, (2), 542-547.
26. Puretzky, A. A.; Geohegan, D. B.; Jesse, S.; Ivanov, I. N.; Eres, G. *Applied Physics A* **2005,** 81, (2), 223-240.

SYNOPSIS, TABLE OF CONTENT

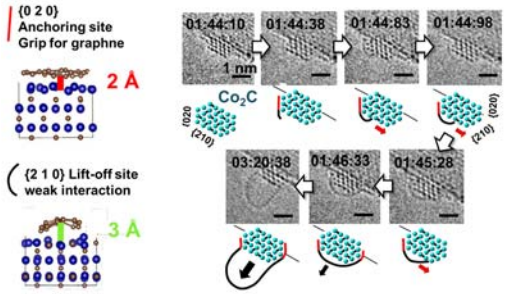

Supporting Information for:

Nucleation of Graphene and its Conversion to Single Walled Carbon Nanotubes

Matthieu Picher, Pin Ann Lin, Jose L. Gomez-Ballesteros, Perla B. Balbuena, Renu Sharma*

*To whom correspondence should be addressed. E-mail: renu.sharma@nist.gov

This PDF file includes:

Materials and Methods
Figs. S1 to S4
Tables S1 to S2
Captions for Movies S1 to S2
References 26 to 31

Other Supplementary Materials for this manuscript includes the following:

Movies S1 to S2

1. Materials and Methods

1.1 High resolution ESTEM

We employ an environmental scanning transmission electron microscope operated at 300 KV, equipped with an image corrector and a charge coupled digital (CCD) camera to record atomic-resolution videos under reaction conditions. Co-Mo/MgO catalyst powder was provided by Prof. Zafar.[1] A drop of catalyst suspension in isopropanol was deposited on a SiC membrane heating chip. The sample was loaded in the microscope and heated to 750 ºC in 10 Pa of O_2. After 15 min, the sample was cooled to room temperature and O_2 flow was terminated. The sample was then heated to 625 ºC and 0.005 Pa of C_2H_2 was introduced. The videos were recorded at a frame rate of 6 s^{-1} at an electron dose of 10^5 nm^2s^{-1} which was not found to significantly affect the growth process, as the same carbon nanotube structures formed in the regions exposed and unexposed by the electron beam.

1.2 DFT calculations

The work of adhesion for the Co carbide surfaces was obtained through density functional theory (DFT) calculations using the Vienna ab initio simulation package, VASP [2-4] with the projector augmented wave (PAW) pseudopotential for the core electrons, plane-wave basis set with a cutoff energy of 400 eV for the valence electrons.

The surfaces were obtained by cleaving the initial structure of the carbide [5] along the planes (020) and (210) using Materials Studio [6]. Four slabs were generated, two with Co or C terminated (020) surfaces and other two with Co or Co-C terminated (210) surfaces. Each of them was composed of 36 Co atoms and 18 C atoms maintaining the stoichiometric ratio Co_2C. The atoms were distributed in six layers, of which the two bottom ones were fixed to simulate the bulk whereas the surface layers were allowed to relax. The dimensions of the simulation cells were 0.9 nm x 0.9 nm x 1.8 nm for the (020) surface and were 0.9 nm x 1.0 nm x 1.8 nm for the (210) surface. Periodic boundary conditions were applied in the x, y, and z directions to resemble an infinitely long slab in the x and y directions but separated from its periodic image in the z-direction by a 1.3 nm vacuum gap. Graphene was modeled as a non-periodic fragment containing five hexagonal rings, so that the lattice could freely accommodate itself to the carbide surface. The graphene fragment has dangling bonds at its rim. Each structure was optimized separately using a conjugate-gradient algorithm to relax the atoms to their ground state. After convergence the graphene was placed on top of each surface at a distance of 0.245 nm and optimized for structural relaxation. The convergence criteria for the electronic self-consistent loop was set to be 10^{-4} eV and for atomic relaxation 10^{-3} eV. The work of adhesion is the energy per unit area necessary to bring two free surfaces into contact. We estimated the work of adhesion from the following relation [7].

$$W_{Adh} = \frac{E_{Co_2C+graph} - (E_{Co_2C} + E_{graph})}{A}$$

The free energies of the individual systems Co_2C and graphene were subtracted from the energy of the combined system and divided by the contact area.

1.3 Structure Identification Method

High resolution images were extracted from the Movie S1 (Fig. S1A) for structural analysis using fast Fourier transformation (FFT or digital diffractogram) (Fig. S1B). Measured d-spacing and angles were matched with known phases containing Co, O, Mg, and C using a software, called CrystalSphere, developed at NIST (https://gitorious.org/crystal-ball-plus). The structures of known phases were retrieved from JCPDS files available at http://www-i.ncnr.nist.gov/icsd/. In the first step, the program uses these files to match all measured d-spacing to the same phase within a specified error and identifies the crystal planes (Table S1). After that, the measured angles between the planes, selected in the first step, are matched. In the final step, a zone axis is assigned. A structure match is assigned only if all (two or more) measured d-spacing, the angles between them, and a common zone axis are matched to a known phase. The structure was further confirmed by matching FFT with a calculated diffraction pattern of the assigned phase (Fig. S1C).

A number of other particles, active for CNT growth (Figure S2) were also measured to ensure the structure identification as the structures of Co_3C and Co_2C are very similar and undistinguishable in certain orientations. Since high resolution images extracted from a video sequence have low signal to noise ratio (SNR) due to short exposure time (0.167 s). As a result measured values for d-spacing and angles obtained from the FFTs are subject to large uncertainties, i.e. ± 0.10 Å for the d-spacings and ± 3 ° for the angles (standard deviations obtained from ten independent measurements). In order to improve the SNR and thereby minimize the measurement errors, twenty consecutive frames were drift-corrected and summed before FFT analysis. As shown in Fig S3, this simple image processing significantly decreased the noise in both the image and the associated FFT. Moreover, we use digital script to find the center of the intensity peaks in the FFTs to further improve the measurement accuracy. As a consequence, the uncertainties drop down to ± 0.03 Å for the d-spacings and ± 0.7 ° for the angle (standard deviation obtained for ten independent measurements). Results are given in Table S2. It is interesting to note that although the FFTs could be indexed for both structures (Table S2), the measured values are much closer to the reported values for Co_2C than for Co_3C. Based on our detailed analysis, the structure of active particles was assigned to be Co_2C and a crystal structure model was built based on the FFT analysis result to identify the surface planes and their structure that defines the nanoparticle geometry (Fig. S4).

1.4 Determination of the nanoparticle surface termination

A graphene sheet is placed at a distance of 0.245 nm from the {020} and {210} facets of Co_2C structure models as shown in Fig. S5A and S6A. After graphene relaxation on the carbide surfaces, calculated distances of the graphene sheet to the Co-terminated {020} (Fig. 3B) and Co-C terminated {210} (Fig. 3D) surfaces are in good agreement with the experimental values (Fig. 2M in main text). On the contrary, a significant discrepancy between experimental and calculated values is observed for C-terminated {020} (Fig. S5B) and Co-terminated {210} (Fig. S6B) surfaces. This confirms that the nanoparticle has Co-terminated {020} and Co-C terminated {210} surfaces. This attribution is also in good agreement with the theoretical simulation reported by Zhao *et al*.[9] which showed that {010} planes are energetically more favored to be Co terminated.

2. Supporting Figures

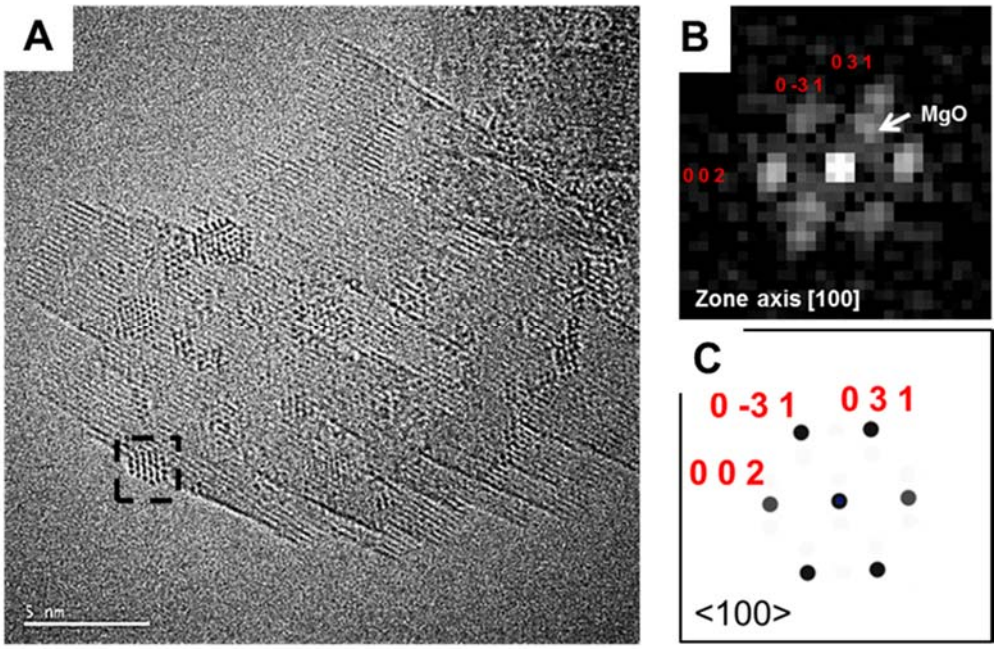

Figure S1. Structure identification. (**A**) An image extracted from Movie S1, with a boxed region containing the particle. Scale bar is 5 nm. (**B**) The FFT of the box area. Measured d-spacing and angle between {031} and (002) of the nanoparticle matched with Co_3C structure oriented along [100] zone axis. Faint spots from MgO (support) are pointed out by an arrow. (**C**) Calculated diffraction pattern of Co_3C in [100] zone axis.

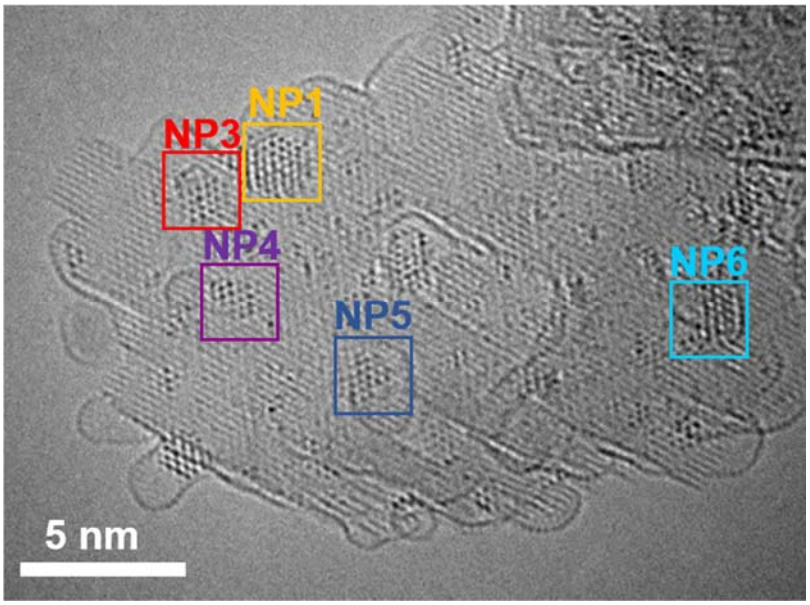

Figure S2. Structure identification. For each labelled nanoparticle, the corresponding measured d-spacings and angles between crystal planes can be found, with the values from JCPDS data source, in Table S2.

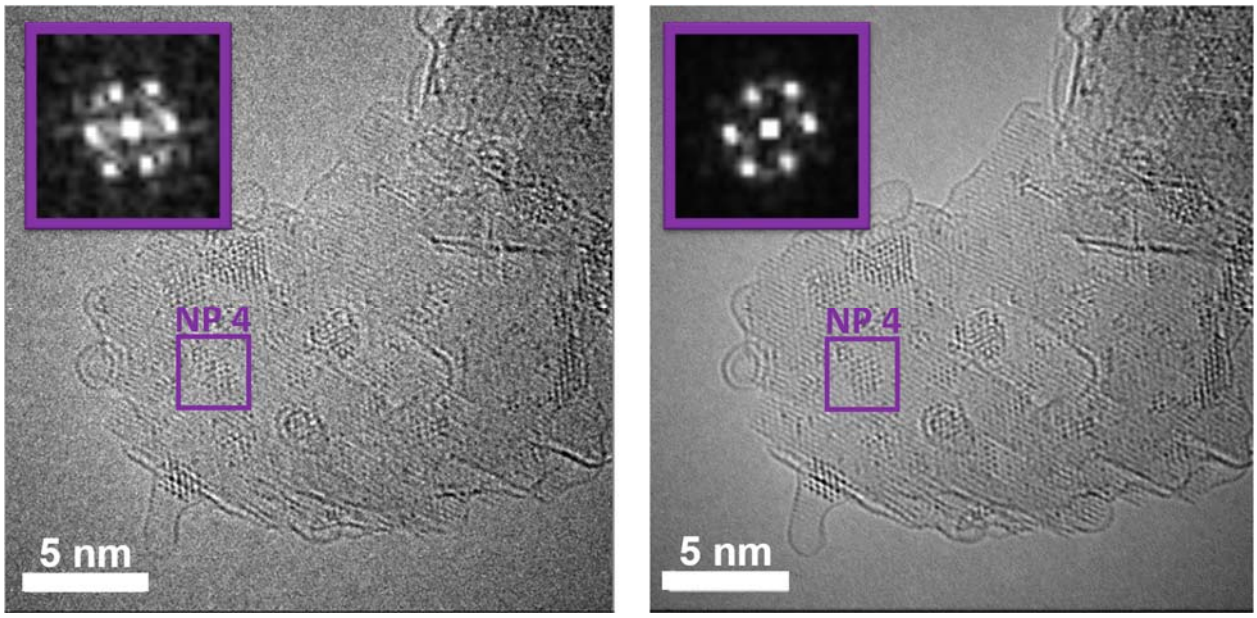

Figure S3. Structure identification. (**A**) Single frame extracted from Movie S1. (**B**) An image after summing 20 drift corrected frames. For each image, the FFT from area marked with purple square (NP4) is presented in the top left inset.

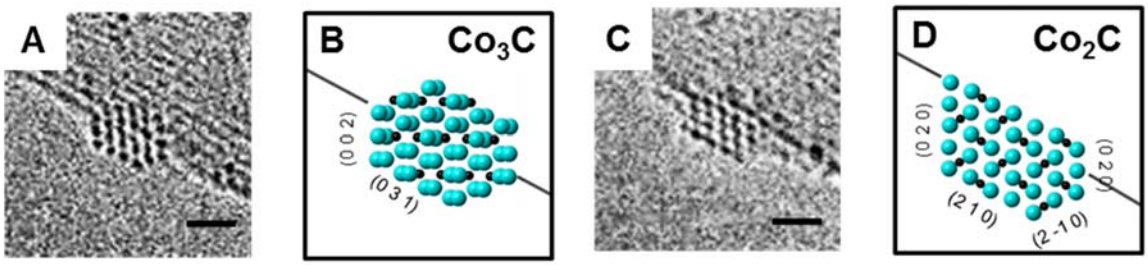

Figure S4. Crystal structure models. (**A**) High resolution TEM image of Co_3C and corresponding structure model showing the indices of the surface planes (**B**). (**C**) High resolution TEM image of Co_2C with corresponding structure model showing the indices of the surface planes (**D**).

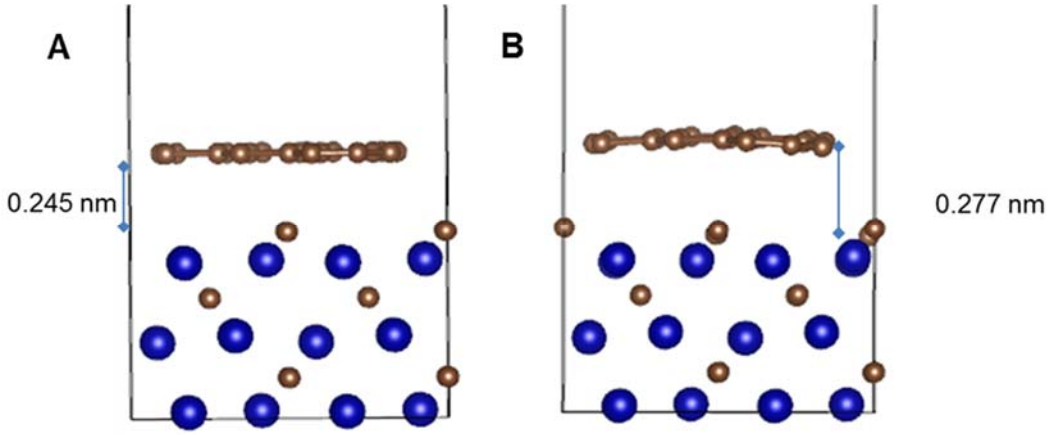

Figure S5. The distances of graphene to C-terminated Co_2C {020} surface before and after relaxation are 0.245 (**A**) nm and 0.277 nm (**B**), respectively.

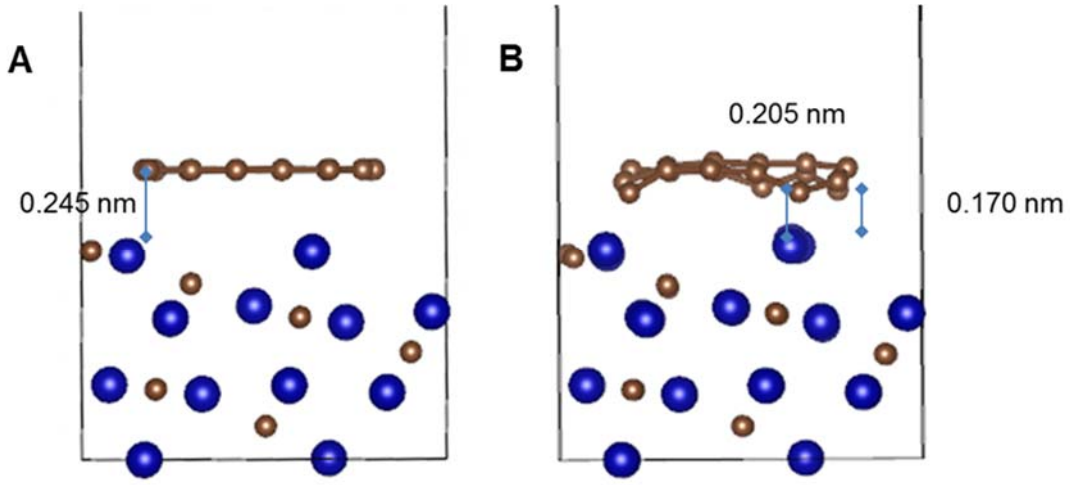

Figure S6. The distances of graphene and Co-terminated Co_2C {210} surface before and after relaxation are 0.245 nm (**A**) and 0.170 nm - 0.205 nm (**B**), respectively.

3. Supporting Tables

Table S1. Comparison of measured d-spacings and angles between crystal planes from the FFT with the values from JCPDS data source (noted as "reference d-spacing" and "reference angles").

Matching Structure	Measured d-spacing (Å)	Reference d-spacing (Å)	Error* (%)	Miller plane	Angle between planes	Reference Angle (°)	Error (°)	Zone axis
Co_3C	1.91	2.01	-4.88	(0 3 1)	0	0		[100]
	2.31	2.23	2.26	(0 0 2)	125.0	117.0	8.0	
Co_2C	2.12	1.99	6.32	(2 1 0)	0	0		[001]
	2.36	2.21	6.64	(0 2 0)	56.4	63.0	-6.6	

* All measurements are given as (mean ± one standard deviation), standard deviations are determined from multiple measurements.

Table S2. Structure determination of different particles during the growth. Comparison of measured d-spacings and angles between crystal planes from the FFT with the values from JCPDS data source (noted as "reference d-spacing" and "reference angles") for the nanoparticles marked P1, P3, P4, P5 and P6 in Figure S2.

NP / Reference	Measured d-spacing (Å)	Reference d-spacing (Å)	Error* (%)	Miller plane	Measured angle (°)	Reference Angle (°)	Error (°)	Zone axis
NP1 / Co_2C	2.36	2.439	-3.4	a: (1 0 1)	a/b 52.4	a/b 56.93	-4.5	
	2.23	2.235	-0.1	b: (2 0 0)	b/c 56.1	b/c 56.93	-0.9	[0 1 0]
	2.40	2.439	-1.5	c: (1 0 -1)	a/c 108.5	a/c 113.86	-5.3	
NP1 / Co_3C	2.36	2.382	-1.4	a: (1 2 1)	a/b 52.4	a/b 58.16	-5.7	
	2.23	2.258	-1.2	b: (0 0 2)	b/c 56.1	b/c 58.16	-2.1	[2 1 0]
	2.40	2.382	0.8	c: (1 2 1)	a/c 108.5	a/c 116.33	-7.8	
NP3 / Co_2C	2.45	2.432	0.9	a: (0 1 1)	a/b 49.2	a/b 56.68	-7.5	
	2.15	2.213	-2.8	b: (0 2 0)	b/c 58.5	b/c 56.68	1.8	[1 0 0]
	2.54	2.432	4.4	c: (0 1 -1)	a/c 107.7	a/c 113.35	-5.6	
NP3 / Co_3C	2.45	2.382	3.0	a: (1 2 1)	a/b 49.2	a/b 58.16	-8.9	
	2.15	2.258	-4.7	b: (0 0 2)	b/c 58.5	b/c 58.16	0.3	[2 1 0]
	2.54	2.382	6.5	c: (1 2 1)	a/c 107.7	a/c 116.33	-8.6	
NP4 / Co_2C	2.44	2.439	0.2	a: (1 0 1)	a/b 53.2	a/b 56.93	-3.8	[0 1 0]
	2.23	2.235	-0.2	b: (2 0 0)				
NP4 / Co_3C	2.44	2.382	2.4	a: (1 2 1)	a/b 53.2	a/b 58.18	-5.5	[2 1 0]
	2.23	2.258	1.3	b: (0 0 2)				

NP5 / Co_2C	2.45	2.432	0.8	a: (0 1 1)	a/b 54.5	a/b 56.68	-2.2	
	2.26	2.213	1.9	b: (0 2 0)	b/c 54.7	b/c 56.68	-2.0	[1 0 0]
	2.37	2.432	-2.4	c: (0 1 -1)	a/c 109.2	a/c 113.35	-4.1	
NP5 / Co_3C	2.45	2.382	2.8	a: (1 -2 1)	a/b 54.5	a/b 58.16	-3.7	
	2.26	2.258	-0.1	b: (0 0 2)	b/c 54.7	b/c 58.16	-3.5	[2 1 0]
	2.37	2.382	-0.3	c: (-1 2 1)	a/c 109.2	a/c 116.33	-7.1	
NP6 / Co_2C	2.35	2.432	-3.2	a: (0 1 1)	a/b 50.8	a/b 56.68	-5.9	[1 0 0]
	2.24	2.213	0.1	b: (0 2 0)				
NP6 / Co_3C	2.35	2.213	6.4	a: (2 0 1)	a/b 50.8	a/b 58.68	-7.9	[0 1 0]
	2.24	2.213	1.2	b: (2 0 -1)				

Table S3. Results obtained from DFT calculations for the work of adhesion between graphene and Co-terminated {020} and Co-C terminated {210}. Four different initial positions of the graphene sheet on the two carbide surface have been tested. Both adhesion processes are favorable, since the combined system (graphene on Co_2C) has lower energy than the individual systems. However, the {020} surface presents a stronger interaction than the {210} surface in all cases. The average work of adhesion values are -26.496 eV nm^{-2} and -14.386 eV nm^{-2} for the {020} and {210} surfaces, respectively.

Energy (eV)	Surface (test 1)		Surface (test 2)		Surface (test 3)		Surface (test 4)	
	(020)	(210)	(020)	(210)	(020)	(210)	(020)	(210)
Co_2C	-359.472	-361.605	-359.472	-361.605	-718.943	-482.148	-718.943	-482.148
graphene	-145.916	-145.916	-145.916	-145.916	-145.916	-145.916	-145.916	-145.916
Combined	-516.268	-512.367	-516.150	-513.897	-876.197	-633.724	-875.036	-634.620
W_{adh} (eV nm^{-2})	-26.737	-11.898	-26.423	-15.654	-27.837	-13.896	-24.986	-16.096

Movie S1. High resolution movie recorded at 0.005 Pa of C_2H_2, and 625 °C, showing multiple catalyst nanoparticles during nucleation (frame rate of 6 s^{-1}).

Movie S2. High magnification movie extracted from Movie S1 showing the atomic scale structure of P2 during graphene nucleation and showing its conversion into a single-walled carbon nanotube.

References

1 Goyal, A., Wiegand, D. A., Owens, F. J. & Iqbal, Z. Synthesis of carbide-free, high strength iron–carbon nanotube composite by< i> in situ</i> nanotube growth. *Chemical physics letters* **442**, 365-371 (2007).

2 Kresse, G. & Furthmüller, J. Efficient iterative schemes for ab initio total-energy calculations using a plane-wave basis set. *Physical Review B* **54**, 11169 (1996).

3 Kresse, G. & Joubert, D. From ultrasoft pseudopotentials to the projector augmented-wave method. *Physical Review B* **59**, 1758 (1999).

4 Blöchl, P. E. Projector augmented-wave method. *Physical Review B* **50**, 17953 (1994).

5 Nagakura, S. Study of metallic carbides by electron diffraction IV. Cobalt carbides. *Journal of the Physical Society of Japan* **16**, 1213-1219 (1961).

6 Materials Studio 4.4

7 Sholl, D. & Steckel, J. A. *Density functional theory: a practical introduction*. (John Wiley & Sons, 2011).

8 Diehm, P. M., Ágoston, P. & Albe, K. Size-Dependent Lattice Expansion in Nanoparticles: Reality or Anomaly? *ChemPhysChem* **13**, 2443-2454 (2012).

9 Zhao, Y.-H., Su, H.-Y., Sun, K., Liu, J. & Li, W.-X. Structural and electronic properties of cobalt carbide Co2C and its surface stability: Density functional theory study. *Surface Science* **606**, 598-604, doi:http://dx.doi.org/10.1016/j.susc.2011.11.025 (2012).